Application of Inertial Instruments for DSN Antenna Pointing and Tracking

D. B. Eldred, N. M. Nerheim, and K. G. Holmes
Guidance and Control Section

The feasibility of using inertial instruments to determine the pointing attitude of NASA's Deep Space Network antennas is examined. The objective is to obtain 1-mdeg pointing knowledge in both blind pointing and tracking modes to facilitate operation of the Deep Space Network 70-m antennas at 32 GHz. A measurement system employing accelerometers, an inclinometer, and optical gyroscopes is proposed. The initial pointing attitude is established by determining the direction of the local gravity vector using the accelerometers and the inclinometer, and the Earth's spin axis using the gyroscopes. Pointing during long-term tracking is maintained by integrating the gyroscope rates and augmenting these measurements with knowledge of the local gravity vector. A minimum-variance estimator is used to combine measurements to obtain the antenna pointing attitude. A key feature of the algorithm is its ability to recalibrate accelerometer parameters during operation. A survey of available inertial instrument technologies is also given.

I. Introduction

Currently, the Deep Space Network (DSN) antennas are pointed using either precision angle encoders mounted at the reflector azimuth and elevation axes, or a Master Equatorial (ME), which optically determines the angular difference between the antenna and a mirror, which is normal to the boresight and attached to an intermediate reference structure (IRS) on the back side of the primary reflector. The ME is more accurate than the angle encoders; thus the 70-m antennas, which have the most stringent pointing requirements, use MEs. The smaller 26- and 34-m antennas, which have less stringent pointing requirements than the 70-m antennas, rely solely on the angle encoders. Even if the encoders or ME were error-free, there would still be pointing errors arising from uncertainty in the modeling of the IRS, caused by gravity, wind, and thermal effects, as well as by parameter errors, nonlinearities, and model truncation. For example, wind and gravity distort the antenna dish-bearing structures as well as the ME tower itself, which causes errors in the virtual reference plane on the dish relative to the ME mirror

plane and thereby alters the antenna boresight. A strategy has been proposed and analyzed [1] which uses the Spatial High Accuracy Position Encoding Sensor (SHAPES) developed at the Jet Propulsion Laboratory (JPL) to measure distortion in the antenna dish. When combined with a maximum-likelihood estimator, the method can be used to determine the best-fit antenna boresight. However, this sensor still has to be referenced to a known and stable reference plane. There are approximately 25 ft of structure between the ME and the front surface of the 70-m antenna, and translation of a pointing attitude at the ME to a pointing attitude at the reflector surface requires an accurate model of this connecting structure, which does not exist. Presently, gravity-induced sag, systematic component errors, and misalignments are largely removed while other structural effects are treated as random errors and are left uncompensated.

The current study was undertaken to investigate the feasibility of using an inertial pointing system to achieve pointing and tracking performance consistent with operation of the 70-m antennas at 32 GHz. The system would ideally function as a "black box" that outputs pointing attitude upon request. It would be mounted unobtrusively close to the front surface of the main antenna reflector (Fig. 1). This location would eliminate the error introduced by uncertainty in the model of the structure between the ME and the antenna surface, and would provide an antenna pointing reference that can be used to steer the antenna or from which SHAPES or another surface-sensing sensor could measure. The system would be required to operate in real time and provide capabilities for both blind pointing and precision tracking. A pointing-vector sensing accuracy of 1 mdeg root mean square (rms) or better over a 10-hr tracking period is used as a performance target in the study and serves as the basis for sorting out the potential inertial instrument candidates. This performance requirement is driven by the narrow radio-frequency beam resulting from 32-GHz operation of the 70-m antennas. Additional factors that were considered include reliability, maintenance requirements, and instrument cost.

The investigation includes both the development and analysis of concepts for determining pointing attitude and an assessment of state-of-the-art instruments. Critical issues include attitude initialization and on-line compensation for pointing system errors throughout antenna tracking periods. It was recognized at the onset of the study that the requirements could not be met easily with the available instruments. However, by using multiple instrument arrays, common-mode rejection, and parameter-estimation processing algorithms in real time, the instrument deficiencies are largely overcome, particularly in the determination of the elevation attitude. Simulation results using representative instrument parameters are analyzed to illustrate the type of performance one might expect using currently available instruments operating in a DSN antenna environment.

II. Concept Overview

The proposed instrument to effect the pointing functions combines three single-axis gyroscopes in a three-axis configuration (Fig. 2), four accelerometers (Fig. 3), and an inclinometer. The gyroscopes are arranged with their sensitive axes aligned along three mutually orthogonal axes, with one gyroscope nominally along the antenna boresight axis and the other two perpendicular to this. The accelerometers are configured as a plane array perpendicular to the antenna elevation axis and with their sensitive axes oriented at right angles to one another. The inclinometer is mounted such that it is sensitive to any tilt from horizontal of the antenna elevation axis.

The gyroscopes constitute the most important part of the inertial instrument. Gyroscopes measure either angular rate in an inertial frame of reference or the integral of this rate; thus their outputs can be integrated to track any change in antenna attitude due to movement from an initial position. However, due to instrument errors, the accuracy of the computed attitude degrades with time, and the gyroscopes must occasionally be recalibrated against a known reference. This can be done, for example, immediately before a tracking sequence.

The proposed scenario for determining the absolute antenna attitude for gyroscope initialization involves determination of the direction of the local gravity vector and the Earth's spin axis in the antenna local coordinate frame. The gravity vector is determined using the accelerometers and the inclinometer. The accelerometers measure the component of gravitational acceleration along their sensitive axes, which varies according to the elevation angle of the antenna. The inclinometer directly measures the tilt of the elevation axis. The direction of the Earth's spin vector is determined by clamping the antenna's elevation and azimuth axes. With the antenna fixed in the Earth local reference frame, the only remaining angular rate is that of the Earth, which is observed in the gyroscope outputs.

The instrument is configured as a strapdown system in a single assembly, i.e., the individual components are rigidly attached to a holding fixture, which in turn is securely attached to the antenna dish and moves with it. The alternative to a strapdown system is one that is mounted

on an inertially stabilized platform. This alternative configuration can offer added accuracy but was not seriously considered because of its far greater expense, complexity, and maintenance requirements.

III. Theory

A. Elevation Determination

The following describes the principle of operation for determining the elevation using the accelerometers. An accelerometer measures the component of acceleration along its sensitive axis and is insensitive to cross-axis accelerations (within limits). This principle can be applied to determine its orientation relative to a local gravity vector, from which an inertial geocentric vertical can be obtained. For example, the ideal accelerometer in a gravitational field shown in Fig. 4 would have as its output

$$y = g \sin(\theta) \tag{1}$$

which can be inverted to yield the elevation angle

$$\theta = \sin^{-1}\left(\frac{y}{g}\right) \tag{2}$$

Here, y is the accelerometer output, g is the local acceleration of gravity, and θ is the angle between the accelerometer and local horizontal. An advantage of using accelerometers for elevation measurement is that they have a wide range of motion; since many high-quality accelerometers are capable of measuring greater than ± 1 g, the effective range for angle measurement is ± 90 deg. A second advantage is that they can be relatively inexpensive, so that several may be used in an inertial measurement system to provide maximum sensitivity and measurement redundancy, with little impact on total cost.

The inclinometer is used to determine how far the accelerometer array deviates from vertical. An inclinometer is a device that directly measures an angle with high accuracy but may have a limited range. This prevents them from being used as alternatives to the accelerometers. In the following analysis, the inclinometer is ignored and the elevation axis is assumed to lie within the horizontal plane. To include the effect of the tilt of the elevation axis would obscure the analysis while not fundamentally changing the algorithms.

The outputs from the four accelerometers shown in Fig. 3 can be written as

$$y_1 = \alpha_1 + (1 + \beta_1) g \sin(\theta) + \nu_1 \tag{3}$$

$$y_2 = \alpha_2 + (1 + \beta_2) g \cos(\theta) + \nu_2 \tag{4}$$

$$y_3 = \alpha_3 - (1 + \beta_3) g \sin(\theta) + \nu_3 \tag{5}$$

$$y_4 = \alpha_4 - (1 + \beta_4) g \cos(\theta) + \nu_4 \tag{6}$$

Here, θ is the antenna elevation angle, y_i is the output signal, α_i is the bias, β_i is the gain factor, and ν_i is the error associated with the ith accelerometer. For the moment, it is assumed that the biases and gains are known quantities, obtained from calibration of the individual accelerometers.

Equations (3) through (6) can be conveniently represented as the single symbolic vector equation

$$y = h(\theta) + \nu \tag{7}$$

where y, h, and ν are 4×1 vectors with obvious connections to the terms in Eqs. (3) through (6).

Since there are four equations but only one unknown, the system is overdetermined. Accordingly, a minimum-variance estimator is used to determine the elevation angle. It may be assumed, for lack of better knowledge of the error distribution, that the errors ν_i are zero mean and uncorrelated, and have variances given by ${\sigma_i}^2$. Then the covariance R of the measurement error vector ν is given by

$$R \equiv E(\nu\nu^T) = \begin{bmatrix} {\sigma_1}^2 & 0 & 0 & 0 \\ 0 & {\sigma_2}^2 & 0 & 0 \\ 0 & 0 & {\sigma_3}^2 & 0 \\ 0 & 0 & 0 & {\sigma_4}^2 \end{bmatrix} \tag{8}$$

The minimum-variance estimate $\hat{\theta}$ of the elevation angle θ minimizes the cost functional

$$J = \frac{1}{2}(y - h(\theta))^T R^{-1} (y - h(\theta)) \tag{9}$$

which amounts to weighting each of Eqs. (3) through (6) according to its expected error variance. Calculus of variations yields the necessary condition

$$\left(\frac{\partial h}{\partial \theta}\right)^T R^{-1}(y - h(\theta)) = 0 \text{ at } \theta = \hat{\theta} \tag{10}$$

Unfortunately, Eq. (10) is nonlinear and cannot easily be solved directly. To make the problem tractable, the equation is linearized about a close solution θ_0 as

$$h(\theta) \approx h(\theta_0) + \frac{\partial h(\theta_0)}{\partial \theta}\,(\theta - \theta_0) \tag{11}$$

Substituting for the four-vector, given by

$$H(\theta_0) \equiv \frac{\partial h(\theta_0)}{\partial \theta} \tag{12}$$

the minimum-variance estimate is obtained, after some algebra:

$$\hat{\theta} \approx \theta_0 \; + \; \left(H(\theta_0)^T R^{-1} H(\theta_0)\right)^{-1} H^T(\theta_0) R^{-1} (y - h(\theta_0)) \tag{13}$$

Owing to the linear approximation used in the estimator, accuracy is assured only in a small neighborhood of the true elevation angle θ, and so the initial guess θ_0 must be "close" to the true angle, or at least close to the estimate $\hat{\theta}$, since θ is unknown. One way to insure this is to apply the algorithm iteratively. Starting with an initial estimate θ_0 for the elevation angle (obtained from encoders or prior knowledge about what θ should be), $h(\theta)$ is linearized according to Eq. (12) to obtain $H(\theta_0)$. Using this quantity, Eq. (13) is used to obtain a better estimate for the elevation angle. This in turn is used as the new starting estimate for the algorithm, and the process is repeated until no further improvement is observed. In practice, the algorithm has been observed to converge after several iterations, reflecting the slow rate of change of $H(\theta)$ as a function of angle θ.

It is possible to obtain an expression for the covariance of the estimate if the measurement errors can be characterized [3]. It is assumed that the error vector ν is gaussian distributed random and zero mean, which is reasonable for independent analog transducers subject to external noise such as the accelerometers. Then the covariance is given by

$$P_\theta = E(\hat{\theta} - \theta)^2 \tag{14}$$

$$= \left(H^T(\hat{\theta}) R^{-1} H(\hat{\theta})\right)^{-1} \tag{15}$$

If for the moment it is assumed that all the accelerometers have zero bias ($\alpha_i = 0$), unit gain ($\beta_i = 0$), and equal error variances ($\sigma_i = \sigma_a$), then it can be shown after some algebra that the expected standard deviation of the estimate is given by

$$\sigma_\theta = \sqrt{P_\theta} = \frac{\sigma_a}{\sqrt{2}\, g} \tag{16}$$

where again, σ_a is the standard deviation of a single accelerometer, g is the acceleration of gravity, and σ_θ is the predicted standard deviation of the resulting angle measurement.

At this point it is appropriate to discuss some of the advantages of the four-accelerometer configuration. First, the expected angle error given by Eq. (16) is independent of elevation angle θ. In other words, the instrument is uniformly sensitive at all attitudes. This is a consequence of having the instruments mounted along orthogonal axes; although it is possible to determine elevation angle with a single accelerometer, the resulting error in the estimate varies with angle and even diverges when the accelerometer is oriented parallel to gravity. Second, the configuration provides for common-mode rejection. In the estimator, the outputs from two accelerometers in a back-to-back pair are essentially subtracted from one another. Thus, any unintended response common to both accelerometers is effectively negated. The advantage of back-to-back instruments goes even one step further by eliminating some nonlinear terms. In general, the most significant nonlinear term in an accelerometer is the quadratic term, commonly referred to as rectification. This term could arise, for example, in a dynamic environment where seismic vibrations were present. Again, since the outputs from the back-to-back accelerometers are essentially differenced in the algorithm, the rectification term nominally disappears and disappears completely if the accelerometers have identical characteristics.

The description of the minimum-variance estimator used to determine elevation angle from the accelerometer outputs is complete except for the corrections required to accommodate deviations of the gravity vector from the true geocentric vertical. However, parameter estimation using an extended Kalman filter is proposed that provides dramatic improvement of the performance. Because of the common-mode rejection, the largest remaining errors in the accelerometer outputs are caused by errors in the biases α_i and the gains β_i. These errors tend to vary from day to day; thus they cannot be removed consistently by means of a one-time calibration. However, as will be shown, it is possible to obtain estimates of them using the accelerometer outputs. The following description illustrates the underlying principle.

For a given antenna elevation, there are four outputs from the accelerometers. The number of unknowns is nine, which includes the elevation angle, four biases, and four gains. The four measurements are linear combinations of the nine unknowns, in a linearized version of the system. The number of unknowns exceeds the number of measurements, so the system is underdetermined.

Now, consider the antenna at a second, different elevation angle. A second unknown is added—the second elevation angle. Four more outputs from the accelerometers are available. These additional outputs are different linear combinations of the unknowns than the first set of measurements since the system equations are linearized about a different angle θ. Thus, at this point the number of unknowns is 10 and the number of measurements is 8. With the addition of measurements at a third elevation, the number of equations will exceed the number of unknowns, and all unknown parameters can be estimated.

In practice, the parameter estimation is implemented using an extended Kalman filter [3]. The components of the state vector at time t_i are defined as the elevation angle, the four biases, and the four gains:

$$x_i \equiv (\theta\ \alpha_1\ \alpha_2\ \alpha_3\ \alpha_4\ \beta_1\ \beta_2\ \beta_3\ \beta_4)_i^T \tag{17}$$

In the extended Kalman filter formulation, it is assumed that the state update and measurement equations can be written as a single-stage transition with zero-mean gaussian distributed random noise inputs:

$$x_{i+1} = x_i + \omega_i;\ E(\omega_i \omega_i^T) = Q \tag{18}$$

$$y_i = h(x_i) + \nu_i;\ E(\nu_i \nu_i^T) = R \tag{19}$$

Here, ω_i is the process noise and ν_i is the measurement noise. An extended Kalman filter for estimating the state in this system is given by

$$\hat{x}_{i+1}^- = \hat{x}_i^+$$

$$(\hat{x}_i^-)_1 = \hat{\theta}_i$$

$$H = \frac{\partial h(x_i^-)}{\partial x} \tag{20}$$

$$M_i = P_i + Q$$

$$P_i = M_i - M_i H_i^T (H_i M_i H_i^T + R)^{-1}\ H_i M_i$$

$$K_i = P_i\ H_i^T R^{-1}$$

$$x_i^+ = x_i^- + K_i(y_i - h(x_i^-))$$

Here, x_i^- is the state estimate before the Kalman filter update, and x_i^+ is the estimate after update; $\hat{\theta}$ denotes the minimum-variance estimate derived earlier, K_i is the Kalman filter gain, M_i is the 9×9 state error covariance matrix estimate before update, and P_i is the covariance matrix after update. Of course, all dimensions are compatible with the nine-element state vector and the four-element measurement vector.

The validity of the extended Kalman filter hinges on whether or not the linearization is performed about the correct trajectory. For this reason, the minimum-variance estimate of the elevation angle $\hat{\theta}$ is used in the filter so that the best possible parameter estimates are used before linearization. In the simulation, the benefit of this modification was observed in the sense that angle estimation is more accurate using the minimum-variance estimate than not using it.

The covariance propagation equations as given in Eq. (20) are well known to be sensitive to small errors introduced from computational errors, and it is a common problem that positive definiteness in the covariance matrices can be lost, which can cause divergence of the filter. To insure against this sort of problem, a square-root algorithm was used to propagate the covariances [2].

The parameter estimation works best when the antenna is rotated through as wide a range of elevation as possible. This suggests an initial calibration to initialize the accelerometers, which is best accomplished prior to the start of a tracking period. The calibration sequence would require the antenna to be elevated from horizontal to vertical. Even during tracking, the changes in elevation which occur are sufficient to allow the filter to significantly improve the accuracy of the elevation estimate.

B. Gyroscope Initialization

In order to obtain the antenna attitude angle using the gyroscopes, the measured angular rates are integrated over time. Errors in the gyroscope outputs, which may include both systematic and random errors, are simultaneously integrated, resulting in corresponding errors in the computed attitude. Thus it is necessary to reinitialize the gyroscopes occasionally to determine their integration constants. To initialize the gyroscopes, the antenna's attitude in inertial space must be known at some instant in time, at which point the offset between the computed attitude and actual attitude can be computed. The offset is then subtracted from all subsequent computed attitudes to provide a more accurate attitude estimate. It is not critical where the antenna is pointed to obtain this initial attitude, since it can be slewed to a desired target afterwards using the gyroscopes and the accelerometers to guide the antenna along its desired trajectory.

Determining the antenna's attitude is equivalent to determining the coordinate transformation between the antenna's local coordinate system and some known reference system, e.g., inertial or Earth-based. The most commonly used transformation is a 3×3 rotation matrix, which is

composed of nine elements that consist of the direction cosines between the coordinate axes in the local system and the corresponding axes in the reference system. An alternative formulation using quaternions has computational advantages for real-time computations [2] and will likely be used in an implementation of the proposed concept; however, quaternions are not used in the analysis presented here and therefore are not discussed further in this article. Of the nine parameters that constitute a rotation matrix, only three are independent. Thus to evaluate the rotation matrix, or equivalently, the antenna attitude, at least three parameters must be determined.

Two of the three required parameters can be determined by establishing the direction, in the antenna reference system, of a vector whose direction is known in the absolute reference frame a priori. For example, the direction of any vector originating from the center of the Earth is specified by the two parameters of latitude and longitude. Once the direction of a second, different vector is known, the coordinate transformation is overspecified and can be estimated by combining the measurements in a minimum-variance estimator. One example of a vector that could be used to determine absolute antenna attitude is the local gravity vector. Its direction can be estimated using the algorithms described in the previous section. A second candidate vector is the Earth's spin vector. This can be determined using the gyroscopes, which fundamentally measure angular rate about their sensitive axes. However, one must be careful to accommodate any rate caused by motion of the antenna relative to the Earth. A third candidate vector is a ground-based optical beacon. The antenna could be pointed towards a beacon whose position is known from a prior survey, using a star tracker in a closed-loop system. This technique has the disadvantage that a star tracker is required and is also subject to errors caused by refraction in the atmosphere. Yet another candidate vector for initialization is a celestial object such as a star or radio source. The primary disadvantage of determining the direction of such a vector is that the antenna must actively track the object to determine its direction; additional disadvantages include errors caused by atmospheric refraction and the necessity for a star tracker (for an optical source).

The proposed scenario for initializing the gyroscopes uses determination of the local gravity vector and the Earth's spin vector to determine the required coordinate transformation. The scenario requires temporarily locking the antenna in its elevation and azimuth axes to hold the antenna rate relative to Earth to zero, at least in a mean sense if seismic vibrations are present, so that the accelerometers and gyroscopes can be averaged over a period of time to obtain the best possible accuracy. It was recognized from the beginning that the requirements on the gyroscopes would be severe to determine the Earth's spin vector with sufficient accuracy for 1-mdeg pointing. It is estimated from the statistical properties of available gyroscopes that the antenna will have to be kept stationary for approximately 15 minutes in order to achieve this level of pointing knowledge. This is a burden on antenna operations which must ultimately be weighed against the disadvantages of alternative initialization strategies such as those utilizing star trackers.

A minimum-variance estimator is used to determine the direction of the Earth's spin axis using the outputs from the three gyroscopes. Figure 5 shows the relative orientations of the antenna local reference frame, the gyroscopes, and the Earth's spin axis. The corresponding measurement equations are

$$\begin{pmatrix} y_1 \\ y_2 \\ y_3 \end{pmatrix} = \begin{pmatrix} \Omega_1 \\ \Omega_2 \\ \Omega_3 \end{pmatrix} + \begin{pmatrix} \nu_1 \\ \nu_2 \\ \nu_3 \end{pmatrix} \tag{21}$$

Here, Ω_i is the component of the Earth's spin vector along the ith coordinate axis, y_i is the rate output associated with the ith gyroscope, and ν_i is the corresponding rate-error term. The gyroscope errors ν_i consist of both random errors such as might be caused by electronic noise, and deterministic components such as those caused by imperfect calibration, drift in gyroscope parameters, uncompensated temperature effects, etc. It is reasonable to assume that since the gyroscopes are identical within manufacturing tolerances, the expected variances of the error terms should be approximately equal, at least on the average:

$$E(\nu_1{}^2) = E(\nu_2{}^2) = E(\nu_3{}^2) = R \tag{22}$$

The corresponding minimum-variance estimate of the Earth spin vector, $\hat{\Omega}$, is found by minimizing the cost functional

$$J = \frac{1}{2R} \sum_{i=1}^{3} (y_i - \Omega_i)^2 \tag{23}$$

from which the components of the spin vector estimate can be obtained

$$\hat{\Omega}_i = y_i \tag{24}$$

Because the measurements are taken along independent axes, the error in the estimate $\hat{\Omega}$ is given, where I is the 3×3 identity matrix, by

$$E(\hat{\Omega} - \Omega)(\hat{\Omega} - \Omega)^T = RI \tag{25}$$

Within one standard deviation, the estimate lies within a sphere of radius $\sqrt{R}$ of the true spin vector, as illustrated in Fig. 6. It can be seen that the angular error in the estimate of the Earth's spin vector is bounded by

$$\sigma_s \leq \frac{\sqrt{R}}{|\Omega|} \tag{26}$$

Here, σ_s is the standard deviation of the angular error in the estimated spin vector.

With knowledge of the Earth's spin vector and the local gravity vector and estimates of their respective errors, it is possible to construct an estimator that combines the local gravity vector with the Earth spin vector to determine the rotation matrix Q which relates the antenna local reference frame to the Earth local frame, i.e.,

$$e_i = Qe_i' \tag{27}$$

Here, e_i is the ith unit vector in the Earth or "unprimed" frame and e_i' is the corresponding unit vector in the antenna or "primed" frame. The rotation matrix Q can be written as the product of two rotations as

$$Q = Q_1 * Q_0 \tag{28}$$

where Q_0 is the known a priori estimate and Q_1 is a rotation matrix involving small angles that needs to be determined. An intermediate "double-primed" reference frame is defined by

$$e_i'' = Q_0 e_i' \tag{29}$$

where components e_i'' consist of a priori estimates of the Earth-based unit vectors e_i. Thus, it is possible to write

$$e_i = Q_1 e_i'' \tag{30}$$

If Q_0 is a close approximation to Q, then Q_1 can be written using a small-angle approximation. Figure 7 shows the "unprimed" and "double-primed" frames, and it can be seen that for small rotations, Q_1 has the form

$$Q_1 \approx \begin{pmatrix} 1 & -\alpha_3 & \alpha_2 \\ \alpha_3 & 1 & -\alpha_1 \\ -\alpha_2 & \alpha_1 & 1 \end{pmatrix} \tag{31}$$

Here, α_i is the rotation angle about the ith coordinate axis in the "unprimed" frame. The rotation angles α_i, and hence Q_1, can be estimated using a minimum-variance estimator that combines the estimate of the Earth spin vector with the estimate for the local vertical. After some algebra, a state-measurement equation can be developed that has the familiar form

$$y = H\alpha + \nu \tag{32}$$

Here, y is a 6×1 vector whose elements consist of the components of the normalized estimated gravity and spin vectors, H is a 6×3 matrix whose elements are functions of the known rotation matrix Q_0, α is a 3×1 vector whose elements consist of the rotation angles α_i, and ν is a 6×1 error vector. Using Eq. (32), the minimum-variance estimator is developed in the usual manner and has the same form as Eq. (13), the minimum-variance estimator for the antenna elevation angle.

The estimator obtained from Eq. (32) remains valid only as long as the linear approximation given by Eq. (31) for Q_1 remains accurate. This will be true only if the initial approximation to the transformation matrix Q_0 is close to the actual transformation Q. A related problem is that the matrix Q computed using Eq. (28) tends to lose orthogonality because of the small-angle approximation made in Eq. (31). The approach used to address these problems is to use an iterative strategy to determine Q, as follows. An initial approximation Q_0 to the rotation matrix Q is made using angle encoder readouts, which provide a very good initial value. The minimum-variance estimator is used to determine the correction term Q_1. From this, the rotation matrix Q is obtained according to Eq. (28). At this point, Q is reorthogonalized. The process is repeated several times, using the most recently calculated Q as the new Q_0.

The covariance of the estimate can be derived analytically, and is given by

$$P = E(\alpha\alpha^T) = \begin{pmatrix} \frac{R_1 R_2}{R_1+R_2} & 0 & 0 \\ 0 & R_1 & R_1\tan(\phi) \\ 0 & R_1\tan(\phi) & R_1\tan^2(\phi) + \frac{R_2}{\cos^2(\phi)} \end{pmatrix} \tag{33}$$

Here, ϕ is the latitude angle of the antenna, R_1 is the variance of the normalized Earth spin vector (in rad^2) and R_2 is the variance of the normalized local gravity vector (again, in rad^2). From Eq. (33), one can determine the accuracy of the estimate as a function of the accuracy with which the spin and gravity vectors are estimated. This can

be used in reverse to determine the requirements on the gyroscopes and the accelerometers, as will be shown below.

C. Slewing and Tracking

Once the gyroscopes have been initialized, the antenna must be slewed into a position that will intersect the desired tracking trajectory. The speed and accuracy with which the antenna can be slewed is governed by a number of factors, including the rate at which the antenna can be moved, the time that can be tolerated to perform a slew, and the buildup of errors caused by gyroscope errors and sampling rate. Tracking a target is virtually identical conceptually to slewing, except that the slew rate is nearly zero because celestial targets remain essentially stationary in an inertial frame.

Since the baseline configuration uses a ring-laser gyroscope (see below), it is considered in the following discussions of slewing and tracking. An optical gyroscope outputs an integrated angle; thus, to obtain the rate used for the Earth spin axis determination, successive outputs must be differenced. A simplified model for the output of a single-axis optical gyroscope at time t_i can be written as

$$y_i = B_i + \epsilon_d t_i + G(1 + \epsilon_g)\theta_i + \eta_i \tag{34}$$

The quantities are defined as: y_i is the gyroscope output at time $t = t_i$, B_i is the bias drift, ϵ_d is the error in the drift rate, t_i is the time elapsed since gyroscope initialization, G is the gyroscope gain, ϵ_g is the error in the gain, θ_i is the total angle through which the gyroscope has rotated about its sensitive axis, and η_i is the measurement noise, which may be taken to be random. In addition, the gyroscope bias B_i is subject to a random-walk phenomenon caused by quantum-mechanical effects or shot noise:

$$B_{i+1} = B_i + \gamma_i \tag{35}$$

Here, γ_i is a random process noise. Equations (34) and (35) govern the growth of errors in a single optical gyroscope. By inspection, the growth of the error terms with time is as follows. Error caused by drift in the bias is a random-walk process and is proportional to $\sqrt{t}$. Error caused by rate drift is proportional to t. That due to gain error is proportional to the change in angle between sampling periods, which is proportional to the antenna slew rate and inversely proportional to the sampling rate. That due to measurement error is proportional to $1/\sqrt{t}$. Figure 8 shows the growth of the error terms with time for a representative optical gyroscope whose parameters are based on conversations with and specifications provided by several gyroscope manufacturers, and are given in Table 1. In this example, the error contribution from the measurement noise dominates for elapsed times less than about 1 second, while the gain error and bias random-walk terms dominate at larger elapsed times. Note that the contribution from gain error at the longer elapsed times can, in general, be reduced by slowing the slew rate until the bias random walk dominates the error.

An additional source of error during slewing and tracking arises from the fact that rotations are not commutative, except in the limit of infinitesimal rotations [4]. Because of this, the trajectory of the antenna must be known in order to correctly interpret the gyroscope outputs; individually integrating the rate outputs from the three gyroscopes will produce an incorrect result. Since the gyroscopes are sampled at discrete times, the antenna trajectory is only approximated. For example, suppose an antenna undergoes an attitude change resulting from successive rotations about two different axes

$$R = R_1(\theta_1) * R_2(\theta_2) \tag{36}$$

If these rotation angles θ_1 and θ_2 are small, then it is possible to make the approximation

$$R_i(\theta_i) \approx I + \Delta_i(\theta_i) \tag{37}$$

where $\Delta_i(\theta_i)$ is linear in θ_i and $|\Delta_i| \leq c|\theta_i|$, where c is some constant that is close to 1. A second, different rotation that gives the identical gyroscope outputs is given by

$$R' = R_2(\theta_2) * R_1(\theta_1) \tag{38}$$

and differs from R by

$$R' - R \approx \Delta_2\Delta_1 - \Delta_1\Delta_2 \tag{39}$$

Substituting the above bound on Δ_i into Eq. (39), one obtains an expression for a bound on the error in the rotation

$$| R' - R | \leq 2c | \theta_1\theta_2 | \tag{40}$$

The accumulated error from n rotations, each of magnitude θ, is thus bounded by approximately

$$| R' - R | \leq 2cn\theta^2 \tag{41}$$

This relation cannot be used directly to determine the error caused by noncommutation of rotations because the constant c depends on the trajectory followed, which depends on the vibration environment of the antenna. The

determination of the antenna vibration environment is beyond the scope of this article, as it requires a simulation that includes the antenna dynamics. Nevertheless, Eq. (41) does illustrate the growth of this type of error; the error is quadratic with rotation angle and linear with the number of rotations. Furthermore, once c is determined, Eq. (31) can be used to specify the maximum allowable angular excursion θ that can be tolerated between gyroscope sampling periods, and consequently, the maximum allowable slew rate and the required sampling rate. For example, using Eq. (41) with $c = 1$, it can be shown that the number of samples n required to perform a 20-deg slew at a rate of 0.1 deg/sec is about 250,000 over the period of the slew, which is 200 seconds. Thus the sample rate is bounded by about 1250 Hz. Since Eq. (31) represents an upper bound, this sample rate is probably faster than it needs to be.

Since the direction of the local gravity vector can be determined and is available, it is reasonable to incorporate this information into yet another minimum-variance estimator that combines it with the attitude estimate obtained from integrating the gyroscope rates. This estimator has essentially the same structure and derivation as that described in Eqs. (27) through (31), but with two differences: first, the estimated boresight of the antenna which is obtained from integrating the gyroscopes is used in place of the estimate of the Earth's spin vector; and second, the gyroscope integration provides additional information consisting of the antenna rotation about its boresight, for use by the estimator. In this case, the covariance of the minimum-variance estimate is given by

$$P = \begin{pmatrix} \frac{R_1 R_2}{R_1 + R_2} & 0 & 0 \\ 0 & \frac{R_2(R_1 + R_2 \sin^2(\phi))}{R_1 + R_2} & \frac{R_2{}^2 \cos(\phi)\sin(\phi)}{R_1 + R_2} \\ 0 & \frac{R_2{}^2 \cos(\phi)\sin(\phi)}{R_1 + R_2} & \frac{R_2(R_1 + R_2 \cos^2(\phi))}{R_1 + R_2} \end{pmatrix} \tag{42}$$

Again, this expression for the attitude covariance can be used to determine instrument requirements. In Eq. (42), the angle ϕ does not refer to the antenna latitude but instead refers to the angle between the antenna boresight and the local gravity vector.

D. Instrument Requirements

In this section, the expressions for the error covariances are used to obtain error bounds for the accelerometers and gyroscopes. These bounds are obtained by requiring that the norm of the attitude covariance matrix P given in Eqs. (33) and (42) be smaller than the required pointing variance.

First the requirements for initialization are considered. The relevant instrument parameters are absolute accelerometer accuracy in μg, and the gyroscope rate accuracy in deg/hr (for example). It can be shown from Eq. (33) that the following inequality holds true:

$$| P | < R_1(1 + \tan^2(\phi)) + \frac{R_2}{\cos^2(\phi)} \tag{43}$$

Specifying that $|P| \leq 1$ mdeg^2, and substituting 1 mdeg = 17.5×10^{-6} rad, requires both that

$$R_1(1 + \tan^2(\phi)) \leq (17.5 \times 10^{-6})^2 \tag{44}$$

and

$$\frac{R_2}{\cos^2(\phi)} \leq (17.5 \times 10^{-6})^2 \tag{45}$$

Recall that R_1 is the angle variance of the normalized local gravity vector; thus, applying Eq. (16) one obtains

$$\sigma_a \leq \sqrt{2} g \cos(\phi) \times 17.5 \times 10^{-6} \tag{46}$$

as a requirement for the accelerometer accuracy σ_a. Substituting for the latitude of the Goldstone complex, ϕ = 35 deg, the accelerometer requirement becomes

$$\sigma_a \leq 20\ \mu g \tag{47}$$

In other words, the accelerometers must be accurate in an absolute sense to better than 20 μg rms. This accuracy applies to the accelerometers after the extended Kalman filter algorithm has been applied to remove gain and bias errors, so the devices actually used may have relaxed specifications compared to Eq. (47).

The required gyroscope accuracy is given by

$$\frac{R_2}{\cos^2(\phi)} \leq (17.5 \times 10^{-6})^2 \tag{48}$$

From Eq. (26), $R_2 = R/\Omega^2$, where $R = \sigma_r^2$ is the variance of the gyroscope rate and Ω is the magnitude of the Earth's spin rate. Thus, the accuracy requirement on the gyroscope rate is given by

$$\sigma_r \leq \Omega \cos(\phi) \times 17.5 \times 10^{-6} \tag{49}$$

$$\sigma_r \leq 2.1 \times 10^{-4} \text{ deg/hr} \tag{50}$$

It must be recognized that the requirements specified above for the accelerometers and gyroscopes represent upper bounds; when errors from both terms occur simultaneously, each individual term must be correspondingly reduced.

Next, the requirements for tracking at the 1-mdeg level are given. It can be shown, after considerable algebra, that the norm of the covariance matrix for tracking given by Eq. (42) is bounded by

$$| P | \leq R_2 \tag{51}$$

or, imposing the condition that $|P| \leq 1$ mdeg^2, one obtains the necessary condition for the gyroscope drift

$$\sigma_\theta \leq 1 \text{ mdeg} \tag{52}$$

This bound σ_θ is the maximum angular error that can be tolerated from the integration of a single gyroscope at a low slew rate. From Eq. (52), the maximum error in tracking is completely determined by the accuracy in the gyroscopes, and the accelerometers play no role in fixing this bound. This reflects the fact that rotation of the antenna about the local gravity vector can only be sensed by the gyroscopes. This does not indicate, however, that the accelerometers do not benefit tracking performance; on the contrary, they help significantly to determine antenna attitude within the elevation plane.

While the requirements presented above are representative of the performance levels needed to satisfy 1-mdeg attitude knowledge, the system is sufficiently complex that these requirements are overly simplistic. In fact, the true performance of the system for a given set of instruments must be determined via simulation, because of the complex interactions among the various estimation algorithms and the mix of stochastic and systematic error sources.

IV. Component Selection

A. Introduction

A large part of the effort in the feasibility study has been focused on collecting data from the various manufacturers on the performance of available and projected state-of-the-art instruments, including gyroscopes, accelerometers, and inclinometers. This information was needed in order to conduct simulations using representative instrument parameters, and also can be used to make preliminary recommendations for component selection. The instruments suitable for the present application were developed primarily to meet the need for precision inertial guidance for missile systems and other military applications, with some development traceable to spaceflight requirements. The inertial instruments are typically integrated into a single package, either as an inertial platform that retains its attitude in inertial space or as a strapdown system that is rigidly secured to the vehicle. Inertial platforms can be more accurate than strapdown systems and are generally used for long-range navigational systems that must maintain precision for long periods of time. Because of the high cost of inertial platforms, however, strapdown systems are favored for the present application.

The primary sources of information concerning the instrument characteristics were the instrument vendors. For the most part, classified sources were not used in the study. An excellent summary of modern inertial instruments is contained in [5].

B. Gyroscopes

1. Overview. Gyroscopes can be classified as either optical or mechanical. In addition to the familiar spinning-wheel gyroscopes, mechanical gyroscopes include devices such as the hemispherical-resonator gyroscope [6] and the experimental magnetic-resonance gyroscope [5], which do not have any moving parts. Because of their more mature status, the only mechanical devices considered here are the spinning-mass gyroscopes. In spite of the notable lack of a rotating component in the optical devices, the term "gyroscope" has been retained for the optical devices.

Descriptions of the spinning-wheel gyroscopes can be found in standard textbooks such as [7]. There are two major classifications of spinning-wheel gyroscopes. Those constrained to precess only about one axis (the "output" axis) are called single-degree-of-freedom (SDOF) or single-axis gyroscopes, while those that can precess about two axes are referred to as two-axis or two-degree-of-freedom devices. This precession is sensed by the instrument and a torque is generated to counter the rotation about the output axis. Extensive research and development has been devoted to all aspects of precision gyroscopes. As a result, the spinning-wheel gyroscope is much more mature than other types, and consequently shows little potential for radical improvements over the current performance levels. The mechanical gyroscopes considered include the SDOF floated gyroscopes, dynamically tuned gyroscopes, and electrostatically suspended gyroscopes.

Optical gyroscopes are less mature than mechanical gyroscopes and at present are characterized by somewhat larger errors. However, the lack of moving parts in the optical gyroscope provides the basis for a number of potential advantages that include lower initial cost, reduced maintenance and cost of ownership, shorter warmup times,

large dynamic range, greater long-term stability, and insensitivity to acceleration, shock, and vibration. The optical gyroscopes include various versions of the ring-laser gyroscope (RLG) [8] and the interferometric fiber-optic gyroscope (IFOG) [9]. Both types are currently undergoing intense development and show the potential for continued improvement in performance. Of the two, the ring-laser gyroscope represents the more mature technology and is widely used on commercial aircraft as well as for military applications. On the other hand, the fiber-optic gyroscopes are theoretically capable of better performance. An IFOG has been chosen for the guidance system of the upcoming CRAF/Cassini Mariner Mark II space mission.

2. Mechanical gyroscopes.

a. The single-degree-of-freedom-floated gyroscope. The single-degree-of-freedom floated gyroscope (SDOFF) consists of a spinning wheel mounted in a sealed cylindrical float with its spin axis perpendicular to the axis of the cylinder. The cylinder is mounted within a case with bearings that constrain its motion to rotation about the cylinder axis. This axis is also the output axis of the gyroscope. The space between the float and the case is filled with a viscous fluid. To minimize acceleration effects, the fluid is selected to provide neutral buoyancy for the float. The gyroscope input axis is mutually perpendicular to the wheel spin axis and the float axis.

In operation, rotation about the gyroscope input axis produces a torque about the output axis. If the gyroscope is configured as rate-integrating, the float angular rate is such that the viscous drag on the float just balances the gyroscopic torque. Thus, the float rotation rate is proportional to the angular rate about the input axis and the angular deflection of the float is proportional to the time integral of this rate. It is common practice to detect float rotation and apply a countertorque to return the float to its null position. The applied torque is proportional to the rotation rate about the input axis and the angular position of the case is found as the integral of this rate.

Development of the SDOFF gyroscopes during the past 40 years has been mainly in response to the inertial guidance needs for aircraft and ship navigational systems and more recently for missile guidance and control. Examples of the results of this effort for the most precise applications include the use of hydrodynamic gas bearings for wheel support and magnetic suspensions of the float output axis. Also, considerable effort has been devoted to the development of a single-species flotation fluid to avoid errors caused by stratification of mixed-polymer fluids. The need for precision pointing and tracking of directed-energy weapons has placed an emphasis on low noise.

Both Charles Stark Draper Laboratories (CSDL), previously the MIT Instrumentation Laboratory [10], and Northrop Corporation [11] have developed SDOFF gyroscopes that appear adequate for the antenna pointing requirements. Typical performance of the fourth-generation gyroscopes are drift stability of 0.0001 deg/hr over a 24-hr period, and rate uncertainty, which is primarily due to the gyroscope electronics, of 1.6×10^{-5} deg/hr. A simplified cutaway drawing of the CSDL Fourth Generation Technology Demonstration Device is shown in Fig. 9.

b. The dynamically tuned gyroscope. The dynamically tuned gyroscope (DTG) is a spinning-wheel gyroscope that avoids the use of temperature-sensitive flotation fluids that is characteristic of the SDOFF. The DTG was developed in the early 1960s for applications that required medium accuracy in moderately severe environments. Successful applications include use for the inertial reference units of the Voyager spacecraft (DRIRU I) and the Magellan spacecraft (SKIRU) [12]. Another DTG is DRIRU II [13] developed by Teledyne for NASA as the NASA "standard" inertial reference unit.

Although development of the DTG is continuing, high-grade DTGs do not match the accuracy of precision SDOFF gyroscopes and probably would not satisfy the antenna pointing requirements. A cross section of the Teledyne DTG is shown in Fig. 10.

c. The electrostatically suspended gyroscope. Development of the electrostatically suspended gyroscope (ESG) [14] began during the late 1950s, and 0.001-deg/hr gyroscope system performance was demonstrated by 1971. The ESG has undergone continued improvement since then. A major attribute of this system, which has found application as an accurate submarine navigational system, is its long-term stability and high precision.

The ESG is a free-rotor system consisting of a metallic sphere that is spun up to about 3600 rev/sec and electrically suspended in a hard vacuum. The operating period is measured in years. The spin axis remains fixed in inertial space and its position relative to the case is determined by pickoffs. The ESG is produced by both Honeywell and Rockwell International. The Honeywell instrument is made with a hollow sphere and the spin axis is measured optically by observation through a window. The Rockwell device is made with a solid sphere whose center of mass is slightly offset from the geometric center, which causes a slight wobble that can be detected optically, thereby facilitating determination of the spin axis.

The ESG is generally regarded as the most accurate gyroscope available for shipboard navigational systems when

used on a stabilized platform. Unfortunately, the performance figures are classified. It is also a very expensive system and for this reason was not considered for the present application.

3. Optical gyroscopes. Optical gyroscopes are based on the Sagnac effect, which predicts that two optical waves traveling in opposite directions around identical closed paths will experience pathlength differences that are proportional to the rotation rate of the closed loop [15]. The process is shown schematically in Fig. 11, in which optical waves are introduced into a circular loop at point A and traverse a common path in opposite directions. If the loop (and point A) rotate in the clockwise direction, the clockwise wave requires a longer time to arrive back at point A than does the counterpropagating counterclockwise wave. It can be shown that the time difference δt for the arrival times of the two waves at point A and the associated pathlength difference δL are given by

$$\delta t = \left(\frac{LD}{c^2}\right)\Omega \tag{53}$$

and

$$\delta L = c\delta t = \left(\frac{LD}{c}\right)\Omega \tag{54}$$

where D is the loop diameter, $L = \pi D$ is the optical pathlength, Ω is the loop rotation rate, and c is the speed of light. A more general derivation that includes noncircular paths shows that LD may be replaced by $4A$, where A is the area enclosed by the optical loop.

The different types of optical gyroscopes use different techniques to measure the rotation-induced pathlength difference. The optical gyroscopes considered here are the ring-laser gyroscope and the interferometric fiber-optic gyroscope, as represented by the JPL fiber-optic rotation sensor (FORS) [16]. The ring-laser gyroscope takes advantage of the lasing characteristics of an optical cavity between two cavity resonance frequencies. For a fiber-optic gyroscope, L is the total length of optical fiber comprising the optical path. The rotation-induced pathlength difference is sensed as an optical phase difference of the two waves. The phase difference $\delta\phi$ is given by

$$\delta\phi = \frac{2\pi\delta L}{\lambda} = \left(\frac{2\pi LD}{\lambda c}\right)\Omega \tag{55}$$

where λ is the optical wavelength.

It is expected that continued development will continue to reduce errors; however, a fundamental limit to performance of optical gyroscopes associated with photon statistics results in irreducible random-walk errors. This limit does not exist for mechanical gyroscopes, whose errors are caused mainly by the electronic processing.

a. The ring-laser gyroscope. A block diagram of a ring-laser gyroscope is shown in Fig. 12. As the ring laser rotates, the Sagnac effect results in an effective pathlength difference, given by Eq. (54), for waves that propagate in opposite directions. The pathlength changes can be quite small. For the present application, which requires sensing a rotation rate as small as 10^{-4} deg/hr to determine the spin axis to within 1 mdeg, Eq. (54) implies a pathlength difference of about 10^{-19} m for a typical RLG with optical loop area $A = 0.01$ m^2. This indicates the very extreme gyroscope sensitivity required and indicates a need to integrate the gyroscope output for a period of time to accomplish initialization.

The wavelength and frequency of the clockwise and counterclockwise waves in RLGs adjust to satisfy the laser resonance condition that requires an integer number (m) of optical wavelengths λ within the optical cavity. Thus, $\lambda m = L$, or using $c = \lambda\nu$, one obtains the frequency difference of the two laser modes with path length difference δL as

$$\nu_+ - \nu_- = \delta\nu = \frac{\nu}{L}\delta L = \left(\frac{4A}{\lambda L}\right)\Omega \tag{56}$$

The frequency difference is detected as interference fringes as portions of the counterpropagating waves combine on an optical detector. One fringe passes a point on the detector during a time interval of $(\delta\nu)^{-1}$. The output from the RLG is the fringe count and is traditionally represented as the angular motion expressed as arcseconds. A ring-laser gyroscope scale factor ($\lambda L/4A$) of about 1.5 arcsec/count is typical.

The fundamental limit to performance of any RLG is associated with statistical fluctuations of spontaneous emissions from the laser. This error mechanism results in "angle random walk," a quantity characterized by the random-walk coefficient. At the present time, RLG performance is nearly at the quantum limit imposed by the photon statistics.

The key error mechanisms that can be suppressed or compensated are bias and scale factor nonlinearity. Bias is the measured rate when gyroscope rotation rate in inertial space is zero. Scale factor, as indicated above, is the

ratio of the gyroscope rotation rate and the indicated output. At low rotation rates, the counterpropagating waves couple together because of light scattered from each wave to produce a dead zone over which the effective output is zero. This phenomenon is known as "lock-in" and represents the major source of scale factor nonlinearity. Various ways to reduce the scattered light and to compensate for lock-in have been developed.

Ring-laser gyroscopes are classified as either two-wave or four-wave devices. The light waves are linearly polarized in two-wave RLGs and circularly polarized in the four-wave types. Various types of two-wave devices have been developed to compensate for lock-in. The most common techniques to overcome lock-in of two-wave RLGs are body dithering and optical-pathlength dithering. In each, an oscillating bias is applied to produce a sensed rate that is larger than the lock-in for most of the dither period. Dither noise, which used to dominate RLG performance, has been reduced to very low levels. Dithered RLGs are produced by Honeywell, Rockwell International, and Kearfott, among others.

The four-wave RLG, which is produced by Litton and marketed as a ZLG (zero lock-in laser gyroscope)[17], uses an optical method to avoid lock-in. The technique that is used to bias the four-wave gyroscope provides for common-mode rejection of the drift and noise caused by the dc optical bias element.

The RLG output is the count of interference fringes that cross the detector. If the readout is not interpolated to indicate a small fraction of a fringe, a "quantization error" results. The dithered instruments generally use a technique that fixes the quantization error at 1/4 fringe. The resolution of the Litton ZLG is about 10^{-3} fringes.

Typical values of the best performance of present day ring-laser gyroscopes are a random-walk coefficient of $2 \times 10^{-4}\,\mathrm{deg}/\sqrt{\mathrm{hr}}$ and bias instability of 3×10^{-4} deg/hr. The projected performance is very near the fundamental limit with a random walk of $5 \times 10^{-5}\,\mathrm{deg}/\sqrt{\mathrm{hr}}$.

If the bias instability can be reduced to less than 10^{-4} deg/hr, the tracking requirements for a 10-hr period can be met by an RLG. The initialization procedure entails holding the antenna at a fixed position for a period of time. If the jitter of the stationary antenna is zero-mean, the projected random walk would permit the required rate accuracy of 10^{-4} deg/hr with an integration time of 15 minutes. During this period, approximately one-tenth of a fringe will cross the detector.

b. The fiber-optic gyroscope. Fiber-optic gyroscopes are classified as passive devices because the light source is not an integral part of the optical path. Unlike the ring-laser gyroscope, the fiber-optic gyroscope is not subject to the lock-in phenomenon. There are two types of fiber-optic gyroscopes, the interferometric fiber-optic gyroscope (IFOG) [18] and the resonant fiber-optic gyroscope (RFOG). The RFOG is presently under development at CSDL and will not be discussed here. The IFOG is under development at a number of universities and industrial houses. The IFOG discussed below is being developed at JPL as the fiber-optic rotation sensor (FORS).

The motivation for developing fiber-optic gyroscopes is that the all solid-state construction has potential for highly reliable devices characterized by low weight, low power and long life. Once developed, fiber-optic gyroscopes are expected to have a distinct cost advantage over other gyroscopes. The FORS, which is the present baseline inertial reference unit for the CRAF/Cassini Mariner Mark II (MMII) space mission, consists of an integrated optic chip to which the fiber coil, edge-emitting laser diode source, and detector are connected. Figure 13 shows a diagram of the JPL FORS.

In contrast to the ring-laser gyroscope, which measures the Sagnac effect due to a single passage around a closed optical path, the interferometric fiber-optic gyroscope measures the Sagnac effect in a fiber coil having many turns. Because the source is not part of the loop, the frequency of both waves remains constant and the Sagnac effect is measured as a phase difference of the two counterpropagating waves. The phase difference is related to the pathlength as shown in Eq. (55). For an N-turn coil, Eq. (55) may be written as

$$\Delta\phi = 2\pi \left(\frac{4NA}{\lambda c}\right) \Omega \tag{57}$$

where A is the area enclosed by a single loop of fiber.

IFOGs may be operated open-loop or closed-loop by compensating the Sagnac phaseshift through the introduction of a nonreciprocal phaseshift of opposite polarity within the fiber loop. A common method to accomplish the phase-nulling effect is to apply the shift at one end of the loop using a technique known as serrodyne phase modulation. In FORS, the effect of phase nulling is read by sampling a part of the counterpropagating beams using a method called optical beat detection. This results in a scale factor differing from that of the RLG, Eq. (56), by only a factor of n, the refractive index of the fiber.

C2

Detector shot noise provides the fundamental limit to the IFOG performance and results in a random-walk error characterized by a random-walk coefficient, as for the RLG. Shot noise is reduced by increasing the optical power on the detector; however, there is an upper limit to the laser power because of errors due to nonlinear optical effects in the fiber.

Rayleigh backscattering results in short-term random noise that is corrected by the use of broadband optical sources, such as the superluminescent diodes or edge-emitting diodes as used in FORS. Error sources associated with long-term bias stability have been identified and are presently undergoing intense study.

The demonstrated random-walk coefficient (RWC) of FORS is close to the quantum limit for the configuration used. With $\lambda = 1.3$ μm, $L = 1$ km, and $D = 0.1$ m, the measured RWC is 7×10^{-4} deg/root hr. The bias instability goal for the MMII application is 10^{-3} deg/hr.

Additional development is required for antenna-pointing applications. The probable approach would be to increase the fiber length and the LD product to provide a RWC comparable to that of the projected value of the RLG. To be useful for the present application, the bias instability must be decreased by at least an order of magnitude.

C. Accelerometers

1. Overview. Accelerometers are needed to determine the local vertical during the initialization step, and are also used to determine antenna elevation. Accelerometers may also be used to measure the tilt of the elevation axis; however, an inclinometer can perform that function more cheaply and accurately.

The heart of an accelerometer is a proof mass that is constrained to move along a single sensitive axis. A variety of ingenious methods have been used to sense the force on the proof mass and to provide an output signal that is proportional to the input acceleration. Nearly all accelerometers operate in a closed-loop configuration, in which movement of the proof mass is sensed and a signal is generated to restore the proof mass to its null position. An exception is the vibrating beam accelerometer, which operates open-loop and senses the acceleration as the change in frequency of force-sensitive vibrating quartz beams.

Accelerometers are commercially available with a wide range of performance and cost. Reported resolution values vary from a fraction of a μg for high-grade navigational instruments to over a hundred μg for more commonplace applications such as construction work. Some of the accelerometers with capabilities sufficient for the proposed antenna pointing application are discussed below.

2. The gyroscope-based accelerometer. The pendulous integrating gyroscope accelerometer (PIGA) has a pendulous proof mass attached to the spin axis of a single-degree-of-freedom mechanical gyroscope. Acceleration along the sensitive axis results in a force on the proof mass and produces a torque on the gyroscope output axis. The gyroscope is mounted on a member that is rotated in response to the gyroscope output signal to produce a gyroscopic torque that balances the torque caused by the input acceleration. The PIGA output signal is proportional to the time integral of the input acceleration.

The PIGA is probably the highest performance accelerometer available. It has undergone continuous development since World War II by CSDL and the MIT Instrumentation Laboratory. It is presently used in high-performance strategic missiles and can serve as a high-resolution gravimeter. The performance of existing PIGAs includes a resolution of better than 10^{-6} g with prospects of a resolution better than 10^{-8} g projected for future instruments. This performance significantly exceeds the proposed DSN antenna application; however, because of its cost, the PIGA is not considered a candidate for the present application.

3. Force-rebalance accelerometers. The general class of force-rebalance accelerometers contains a proof mass supported by a flexure and constrained to move along a single axis. The position of the proof mass is detected and the mass is restored to its null position by a rebalance force generated by a control loop. The current in the control loop, which is proportional to the input acceleration, provides the output signal. Performance characteristics include the instrument resolution as well as long-term and short-term errors in the bias and gain parameters. As discussed above, the values of the gain and bias parameters may be estimated prior to and during normal operation by using the minimum-variance estimators and extended Kalman filtering algorithms. When this is done, the uncompensated random variations of the bias and gain determine the accuracy of the instrument.

Manufacturers of force-rebalance accelerometers include Bell Aerospace, Textron, Incosym, Kearfott, Litton, Northrop, Rockwell International, Sundstrand, and Schaevitz. Many instruments in this category, which feature a resolution that varies from 1 μg to about 10 μg, meet the requirements for the present pointing application.

4. Vibrating-beam accelerometers. The basic sensing element of the vibrating-beam accelerometer (VBA) is a force-sensitive, vibrating quartz crystal beam that changes its resonant frequency in response to axial tension and compression. Forces are derived from accelerations applied to a pendulously supported proof mass. The proof mass is restrained along the sensitive axis by two quartz beams so that one beam is placed in tension and the other in compression as a result of acceleration. The VBA output signal is proportional to the frequency difference of the two beams. The "push-pull" arrangement of the quartz beams results in common-mode rejection of most of the error sources. A schematic of the VBA [19], which operates open-loop, is shown in Fig. 14.

Acceleration on the VBA's flexure-mounted proof mass places one of the vibrating quartz beams in tension and another in compression. The VBA output is the difference in frequency of the two beams. Thus, the crystal beams and oscillator circuits replace the torquer coils, magnets, and capture electronics of the conventional force-rebalance accelerometer.

The VBA has been under development at the Kearfott Division of the Singer Company (now the Astronautics Corp. of America). Short-term bias stabilities of 1 μg and scale factor stabilities of 1 part per million (ppm) have been demonstrated with the VBA. This performance is well within the requirements of the present application; however, the instrument is not yet available commercially.

D. Inclinometers

The purpose of an inclinometer in the present application is to measure the level of the elevation axis. Common inclinometers make use of force-rebalance accelerometers or the level assumed by a liquid in a suitable enclosure. One simple concept for an inclinometer is based on the carpenter's bubble level. Spectron Glass and Electronics markets a precision version of the bubble concept as an "Electrolytic Tilt Sensor." These units are one-piece glass enclosures partially filled with an electrolyte and constructed with platinum terminals and contacts that form two arms of an electrical circuit. Part of each arm includes the electrolyte as a resistive element. As the sensor is tilted and electrolyte flows from one side to another, the resistance of one arm increases while the other decreases. This change is sensed as a voltage change. The most precise model covers the range of $\pm 1/2$ deg with resolution of less than 1 mdeg. A disadvantage for the present application is that the high precision of the sensor is only available when the inclinometer is mounted precisely "on top" of the elevation axis. As the antenna is elevated, the sensor rolls away from its preferred position, and the accuracy decreases. It would be necessary to use the inclinometer on a gimbal to achieve maximum resolution.

Inclinometers that use dielectric liquids as an integral part of the device are also offered by Schaevitz. A change in angle is measured as a change in capacitance between two plates as the liquid flows to a new position between the plates. The resolution is about 1 mdeg and null repeatability is 5 mdeg. The total angular range is ± 60 deg.

Inclinometers that use closed-loop force-rebalance linear accelerometers are available from a number of vendors. For example, inclinometers with a resolution of 0.1 arcsec and a total range of ± 90 deg are offered by Schaevitz and Sundstrand. The output offset at zero tilt can reach 50 mdeg for the 90 deg range and 2 mdeg when the range is decreased to ± 1 deg.

E. Recommendations

Currently, the best mechanical gyroscopes outperform the best optical gyroscopes. The single-degree-of-freedom floated gyroscope and the electrostatically suspended gyroscope are both mechanical devices that appear capable of satisfying the requirements for inertial pointing. However, optical gyroscopes enjoy continued improvement through intense development, and are expected to surpass the mechanical gyroscopes in performance in the near future. In contrast, the mechanical devices represent a mature technology, and dramatic improvements in performance are unlikely to occur. In anticipation of these future developments, ring-laser gyroscopes have been chosen in the baseline for the inertial instrument. Optical gyroscopes potentially have additional advantages over mechanical gyroscopes, including lower initial cost, greater reliability, and immunity to vibration and gravity loading.

A number of force-rebalance accelerometers appear to be capable of inertial pointing. These devices are relatively inexpensive, off-the-shelf items. Stability of the accelerometer parameters remains a concern since the extended Kalman filter is limited in its ability to estimate rapidly changing instrument parameters. Another concern is the level of hysteresis that might be encountered during the course of antenna tracking. Vibration levels on the antenna and electronic noise also have to be addressed. Even if some unforeseen difficulties rule out the use of available force-rebalance accelerometers, the emerging vibrating-beam accelerometer, when it becomes available, should be a viable option.

Small-angle inclinometers of various types are available, so no specific recommendation is made. There is a problem that the inclinometers lose accuracy when rotated about

their insensitive axes. This would occur, for example, when the antenna elevation was changed. A solution to this problem has been developed which involves mounting the inclinometer on a simple single-axis pendulum-stabilized platform.

V. Simulation Results

Simulations were conducted to illustrate the behavior of the algorithms presented in the article and to predict the performance of inertial instruments, given a set of representative instrument parameters. The simulations were written in Pro-Matlab by The Mathworks, a well-known commercial software product that uses matrices as its fundamental data type, and were run on a Sun 3/60 desktop workstation.

The gyroscope parameters used in the simulations were previously given in Table 1, and the accelerometer parameters are summarized in Table 2. These instrument parameters are fictitious in the sense that they do not correspond to any specific devices, but instead reflect "typical" parameters for current or projected near-term state-of-the-art devices, based on conversations with and data sheets provided by the manufacturers. The purpose of the simulations is to illustrate the feasibility of an inertial pointing system, not to evaluate specific instruments.

The first two simulations, shown in Figs. 15 and 16, illustrate the behavior of the extended Kalman filter which is used to estimate the accelerometer parameters. For this example, the antenna is rotated in elevation from horizontal to vertical. The initial bias and gain errors were initialized with a random-number generator which assigned them values with standard deviations of 100 μg and 100 ppm rms. The two figures show that even with this level of initial error, the bias and gain parameters for this example can be estimated with an accuracy much smaller than 1 μg following the antenna rotation.

Figure 17 illustrates the performance of the elevation-estimation algorithm that can be expected when the antenna is tracking a target. It is assumed that the antenna is located at the same latitude as the antenna complex at Goldstone, and that the tracked object is inertially stationary and elevated 45 deg from the Earth's equator. The tracking period is set at 10 hr. At the beginning of the tracking period, the accelerometer bias and gain errors are set to zero, reflecting the fact that these parameters are initially known from the previous calibration using the extended Kalman filter. However, the accelerometer model that was chosen allows random walk in the bias and gain parameters. The extended Kalman filter successfully estimates these parameters during target tracking, resulting in elevation error smaller than about 2 μrad (0.1 mdeg). The results are impressive but it must be recognized that several factors which would degrade the accuracy have not been accounted for, including seismic vibrations, accelerometer misalignments, nonlinearities, and electronic noise.

The final two simulations shown in Figs. 18 and 19 illustrate the tracking performance of the entire inertial instrument. Again the antenna is assumed to be located at Goldstone, and the target is inertially stationary and elevated 45 deg from the Earth's equator. Fig. 18 shows the tracking performance in terms of boresight error when only the gyroscopes are used to integrate attitude. The nearly linear growth of error with time indicates that the predominant source of error in this case is the rate-bias error, which is typical of gyroscopes. In Fig. 19, the accelerometer and inclinometer measurements were incorporated into the attitude determination using a minimum-variance estimator to combine the outputs with those of the gyroscopes and the extended Kalman filter to determine antenna elevation. The results demonstrate reduced antenna boresight error, particularly during the middle of the 10-hr tracking period when the antenna is closest to vertical, and thus the elevation determination is nearly redundant with the gyroscope output.

VI. Summary

A system using inertial instruments for pointing of the Deep Space Network antennas has been described. The proposed configuration includes a three-axis gyroscope, four accelerometers, and an inclinometer in a strapdown system. The system can be used both to initialize the antenna pointing attitude and to track an object for prolonged periods of time.

The concept for initializing the gyroscopes requires determination of the local gravity vector and the Earth's spin axis in the antenna local coordinate frame. The gravity vector is determined using the accelerometers to measure elevation angle and the inclinometer to measure cross-axis elevation. An advanced algorithm employing both a minimum-variance estimator and an extended Kalman filter is used to combine the measurements to determine elevation angle, and also to estimate instrument parameters, including biases and gains, while the instrument is in operation. The Earth's spin axis is determined using the gyroscopes, with the antenna held stationary.

Once the antenna attitude is known, it can be slewed to a desired target and held there by using the gyroscopes to

integrate angular rate to obtain attitude and using knowledge of the local vertical to augment this estimate, again combining the measurements in a minimum-variance estimator.

The article continues with a survey of available state-of-the art technology, and makes recommendations towards component selection. In particular, the ring-laser gyroscope appears attractive as the candidate gyroscope, and relatively inexpensive accelerometers appear to fulfill the elevation-determination requirements. The article concludes with a sampling of the simulation results illustrating the functions and performance of an idealized instrument on a DSN antenna. The results show pointing performance close to 1 mdeg, indicating that this level of performance may be possible, though not necessarily easy to achieve, with an inertial instrument.

References

[1] R. E. Scheid, "Precision Pointing Compensation for DSN Antennas with Optical Distance Measuring Sensors," *TDA Progress Report 42-97*, vol. January–March 1989, Jet Propulsion Laboratory, Pasadena, California, pp. 127–140, May 15, 1989.

[2] J. R. Wertz, editor, *Spacecraft Attitude Determination and Control*, Boston: D. Reidel Publishing Company, 1984.

[3] A. E. Bryson and Y. C. Ho, *Applied Optimal Control*, Washington, D.C.: Hemisphere Publishing Company, 1975.

[4] H. Goldstein, *Classical Mechanics*, Dallas: Addison-Wesley Publishing Company, 1950.

[5] R. R. Ragan, editor, "Inertial Technology for the Future," *IEEE Transactions on Aerospace and Electronic Systems*, vol. AES-20, no. 4, pp. 414–440, July 1984.

[6] E. J. Loper and D. D. Lynch, "Projected System Performance Based on Recent HRG Test Results," *Proceedings of the IEEE/AIAA 5th Digital Avionics Systems Conference*, Seattle, Washington, October 31–November 3, 1983.

[7] P. H. Savet, editor, *Gyroscopes: Theory and Design*, New York: McGraw-Hill, 1961.

[8] W. W. Chow, J. Gea-Banacloche, L. M. Pedrotti, V. E. Sanders, W. Schleich, and M. O. Scully, "The Ring Laser Gyro," *Reviews of Modern Physics*, vol. 57, no. 1, pp. 61–104, January 1985.

[9] S. Ezekial and H. J. Ardity, editors, *Fiber-Optic Rotation Sensors*, Berlin, Heidelberg, and New York: Springer-Verlag, 1982.

[10] C. Kochakian, R. McKern, and J. Negro, "Performance Characterization of Low Noise Gyro," Thirteenth Biennial Guidance Test Symposium, Central Inertial Test Facility, Holloman AFB, New Mexico, August 1987.

[11] *The GI-G6G-PMM: A Permanent Magnet Rate Integrating Gyro*, Northrop Precision Products Division, Company Brochure D00017, 1989.

[12] C. O. Swanson, J. Kass, and A. Greiner, "Line-of-Sight Stabilization for the Dynamic Magellan Spacecraft," *12th Annual AAS Guidance and Control Conference*, AAS 89-045, Keystone, Colorado, February 4–8, 1989.

[13] R. B. Irvine and J. W. Ritter, "DRIRU II: The NASA Standard High Performance Inertial Reference Unit," *Annual Rocky Mountain Guidance and Control Conference*, AAS 79-021, Keystone, Colorado, February 24–28, 1979.

[14] R. R. Warzynski and R. L. Ringo, "The Evolution of ESG Technology," *Proceedings of the AGARD Conference on Inertial Navigation Components and Systems*, Paper 13, October 2–5, 1972.

[15] G. Joos, *Theoretical Physics*, 2nd edition, New York: Hafner Publishing Co., 1950.

[16] R. Bartman, B. Youmans, and N. Nerheim, "Integrated Optics Implementation of a Fiber Optic Rotation Sensor: Analysis and Development," paper 719-19, *SPIE Proceedings*, vol. 719, Cambridge, Massachusetts, September 21–26, 1987.

[17] M. Fernandez, R. Ebner, and N. Dahlen, "Zero-Lock Laser Gyro," *12th Annual AAS Guidance and Control Conference*, AAS 89-024, Keystone, Colorado, February 4–8, 1989.

[18] V. Vali and R. W. Shorthill, "Fiber Laser Gyroscopes," *SPIE*, vol. 77, pp. 110–115, 1977.

[19] W. C. Albert, "Vibrating Quartz Crystal Beam Accelerometer," *ISA 28th International Instrumentation Symposium*, vol. 28, no. 1, pp. 33–44, 1982.

Table 1. Parameters used to simulate gyroscope behavior

Quantity	Value	Comment
Angle random walk	$(0.1)^2$ mdeg^2/hr	Gaussian distributed error
Drift uncertainty	0.1 mdeg/hr 0-p	Systematic error may be reduced via parameter estimation
Scale factor uncertainty	5 ppm	Systematic error may be reduced via parameter estimation, but error is small except during slew
Resolution/noise	0.1 mdeg 0-p	Measurement error effect is reduced by averaging data over time

Table 2. Accelerometer parameters used for simulating elevation determination

Quantity	Value
Accelerometer noise	$(1.5\ \mu g)^2$
Angle process noise	$(20$ mdeg$)^2$/sec
Bias process noise	$(100\ \mu g)^2$/10 hr
Gain process noise	$(100\ \mu g)^2$/10 hr
Time step used for simulation	10 hr/450

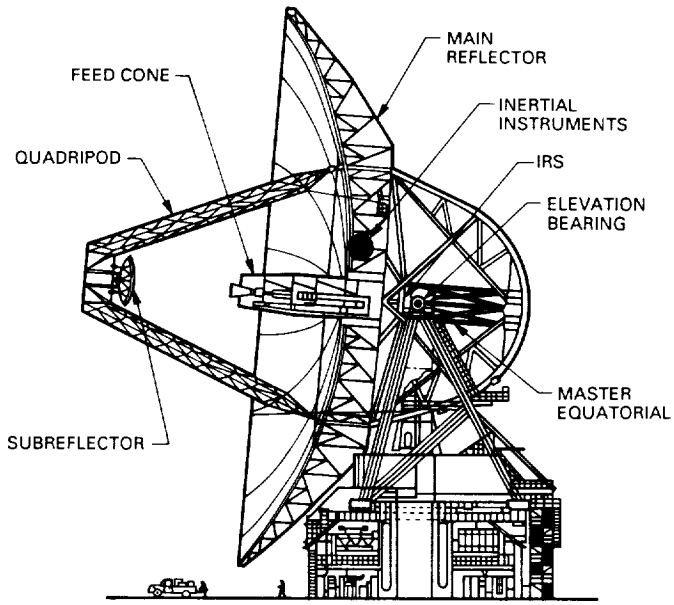

Fig. 1. A 70-m DSN antenna showing potential location of inertial instrument package.

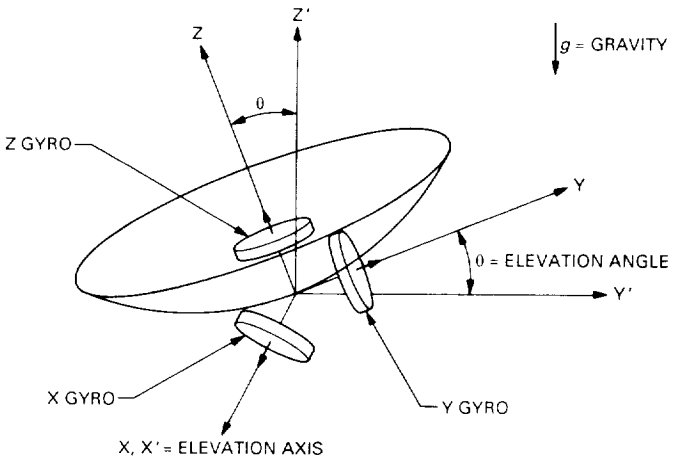

Fig. 2. Orientation of gyroscopes on antenna.

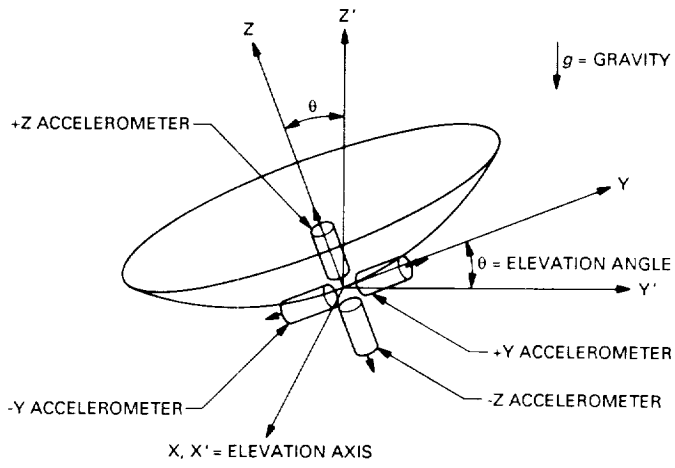

Fig. 3. Orientation of accelerometers on antenna.

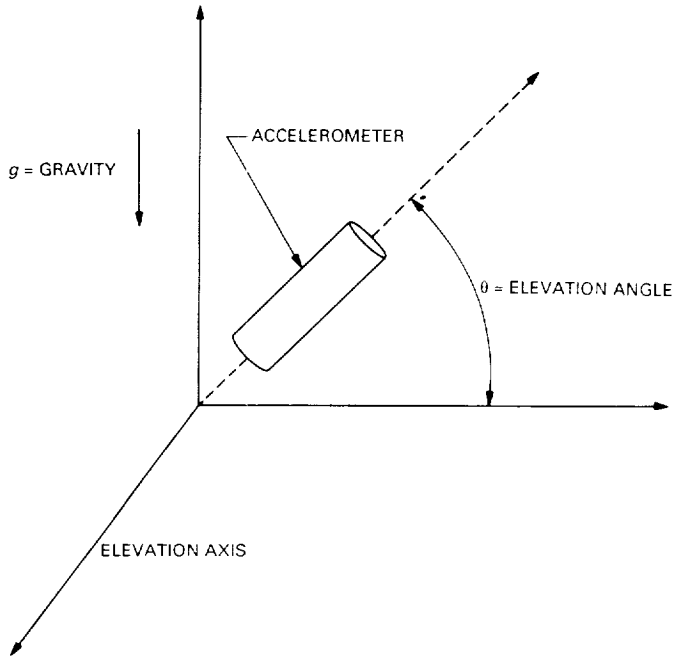

Fig. 4. Single accelerometer under the influence of gravity. Output depends on the angle between the accelerometer sensitive axis and the gravity field.

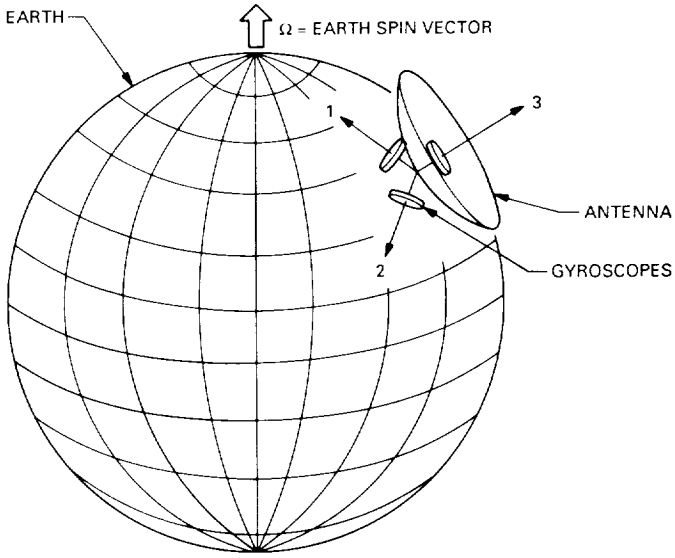

Fig. 5. Orientation of antenna and gyroscopes with respect to the Earth and its spin vector.

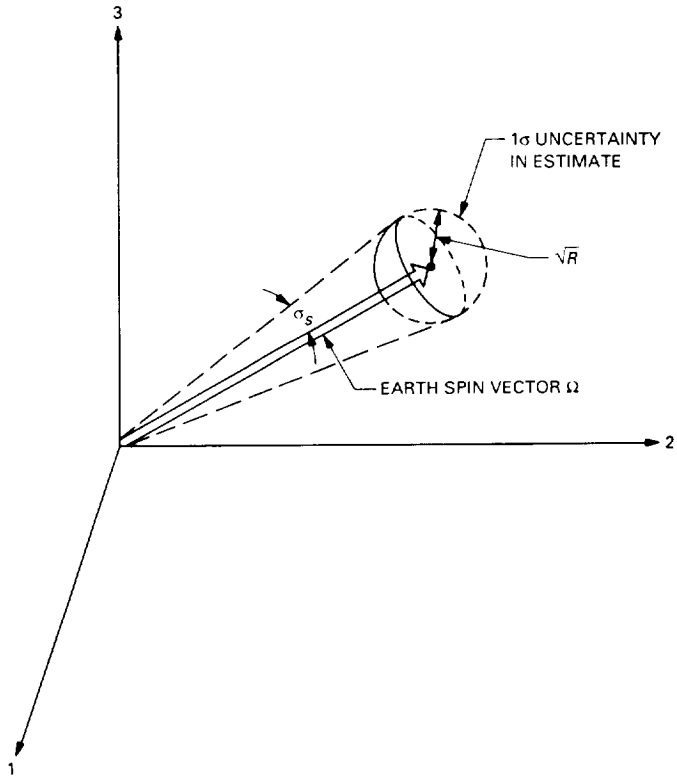

Fig. 6. Uncertainty in the estimate of the Earth's spin vector determined from a minimum-variance estimator.

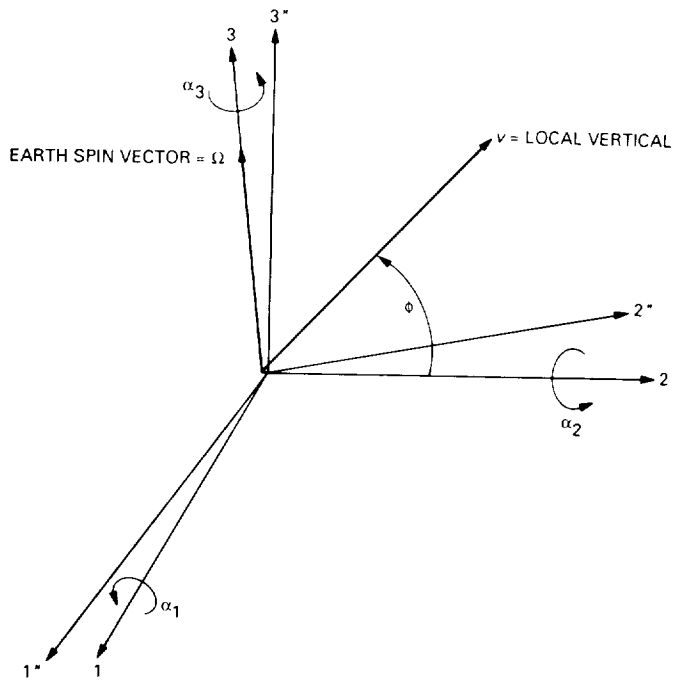

Fig. 7. Coordinate system for definition of small angle corrections. The unprimed frame is attached to Earth, and the double-primed frame is attached to the antenna.

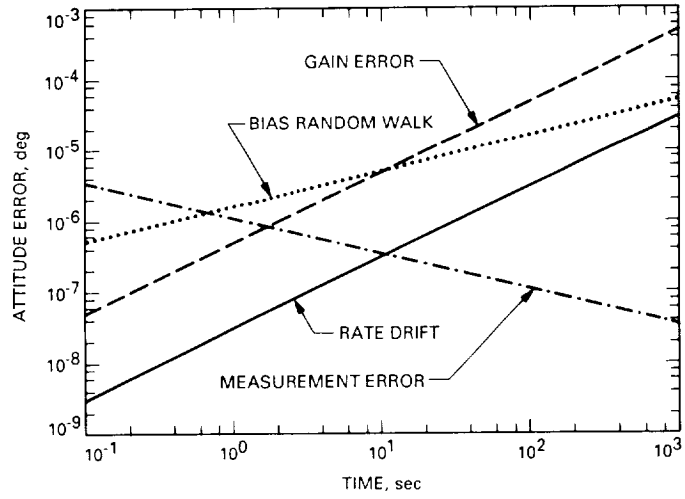

Fig. 8. Summary of error growth terms resulting from integration of a gyroscope.

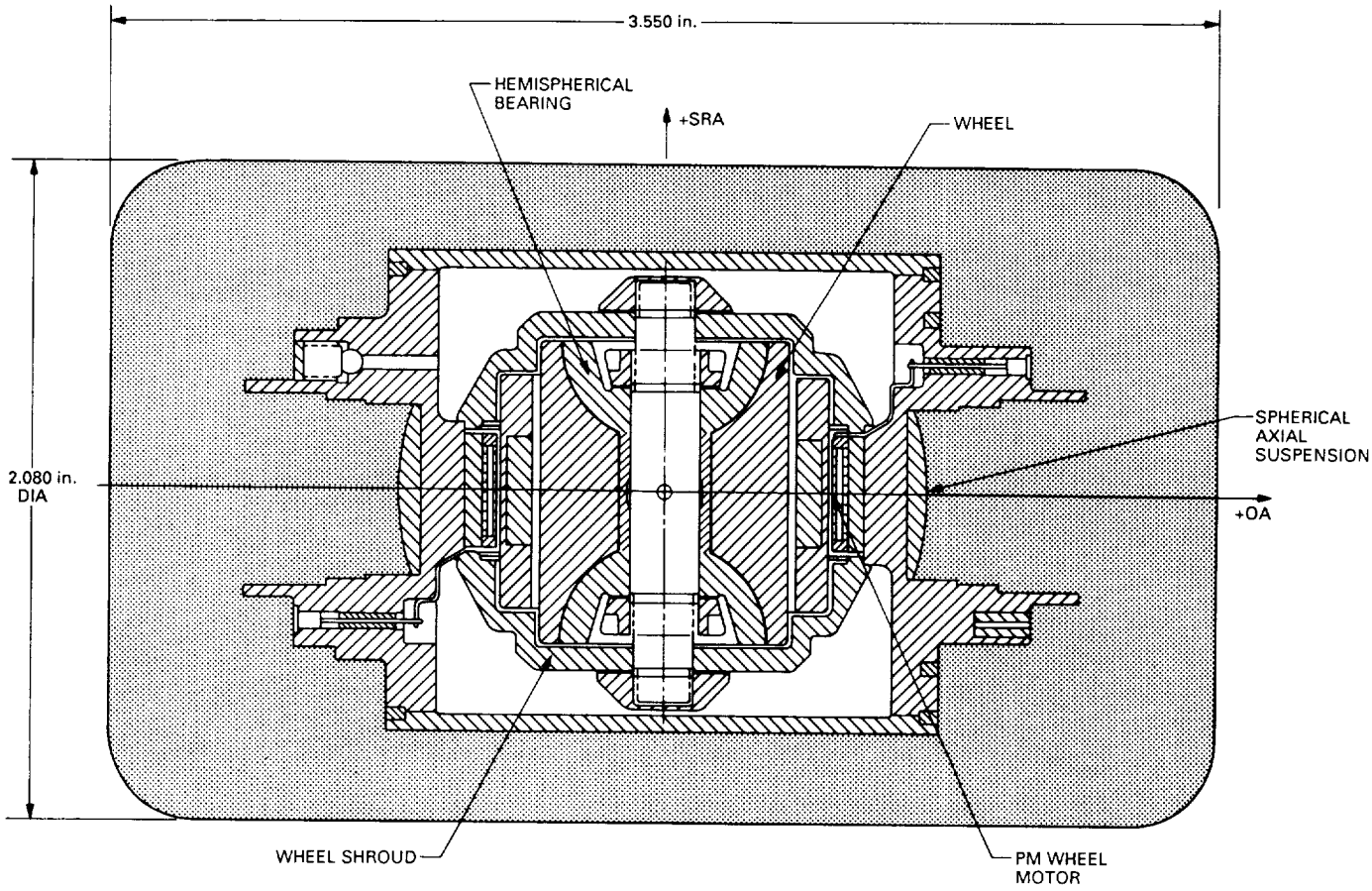

Fig. 9. Simplified drawing of a CSDL fourth generation single-degree-of-freedom floated (SDOFF) gyroscope.

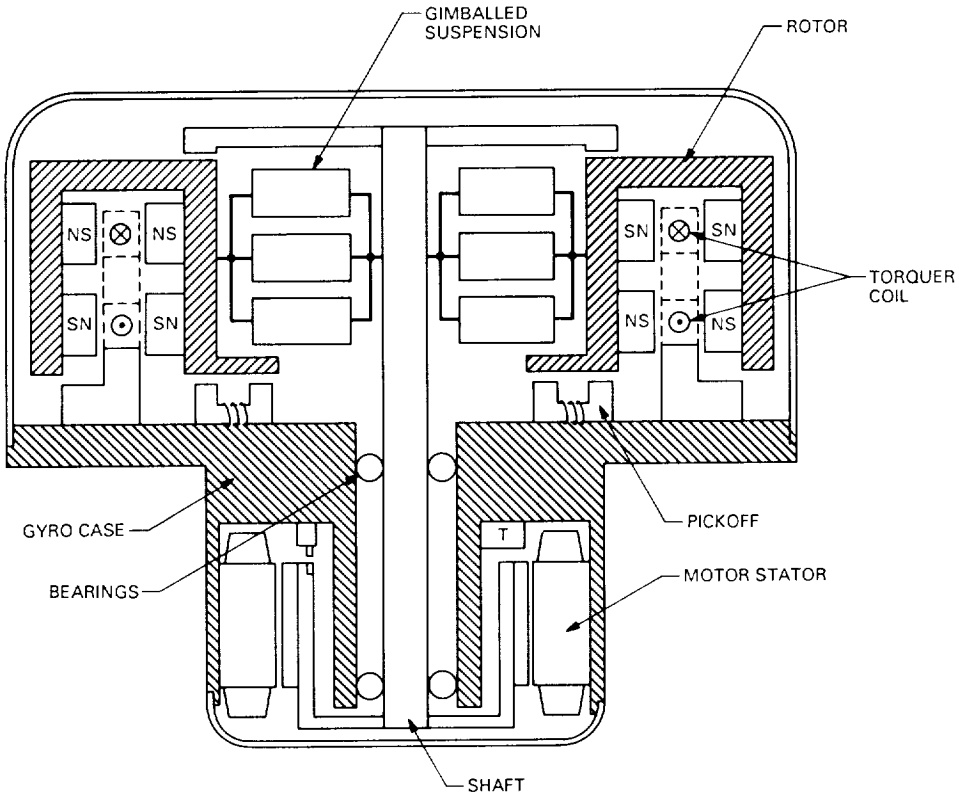

Fig. 10. Cross section of Teledyne's dynamically tuned gyroscope that is used in the NASA-developed dry rotor inertial reference unit (DRIRU II).

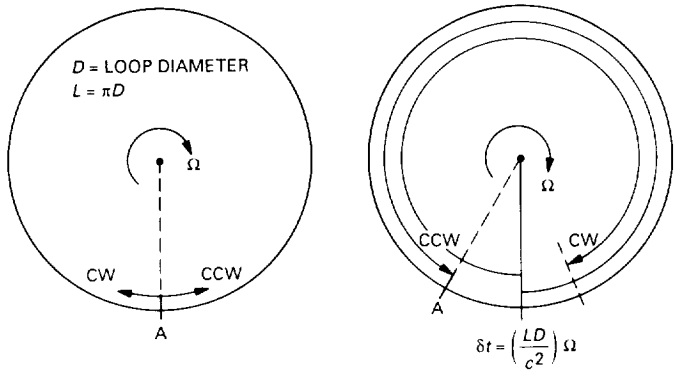

Fig. 11. The Sagnac effect. Optical waves launched in the same direction as the loop rotation require a longer time to complete a revolution than do the counterpropagating waves.

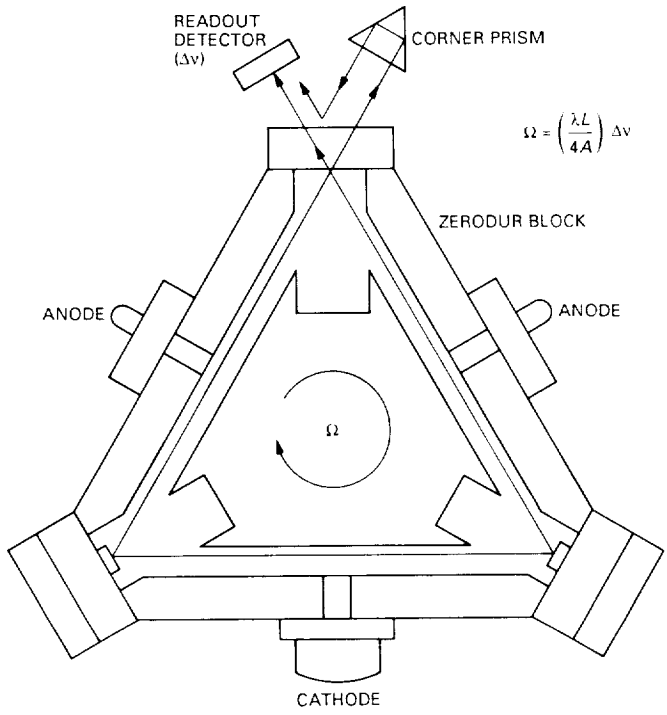

Fig. 12. A ring-laser gyroscope (RLG). Gyroscope rotation changes the optical frequency of counterpropagating waves.

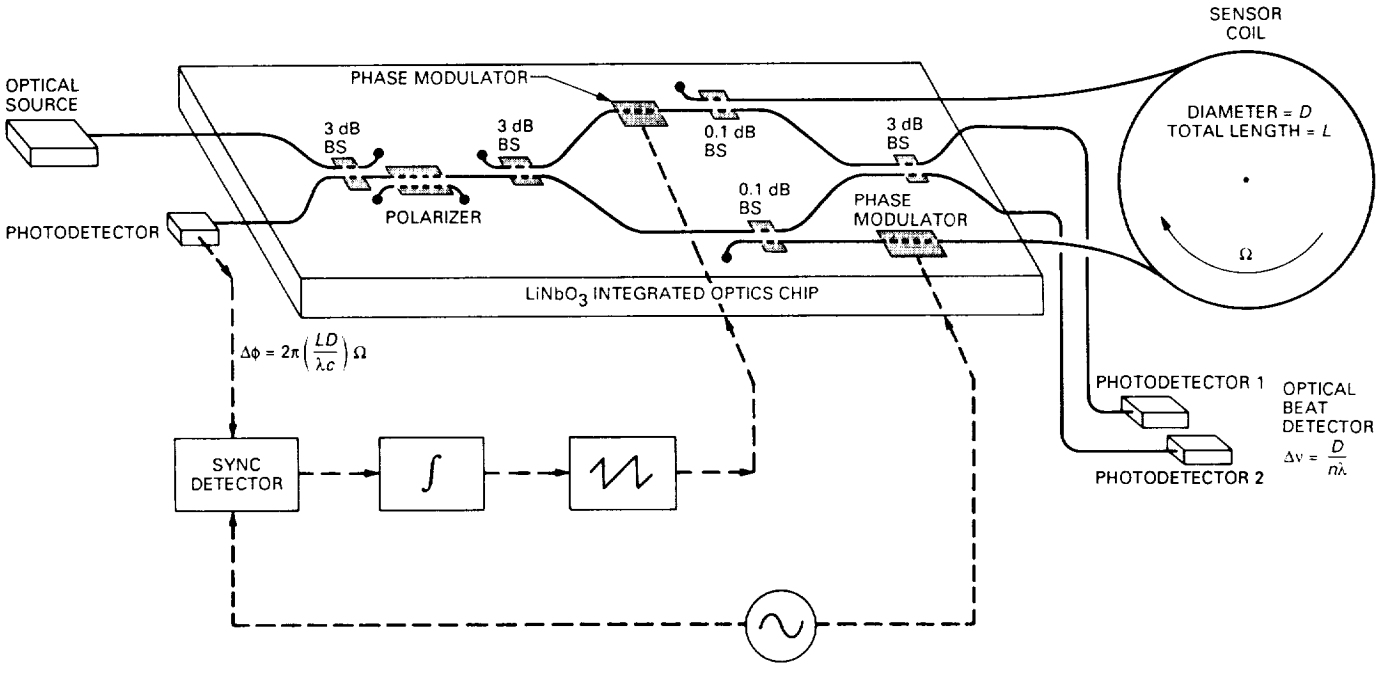

Fig. 13. The fiber-optic rotation sensor (FORS), a fiber-optic gyroscopic under development at the Jet Propulsion Laboratory.

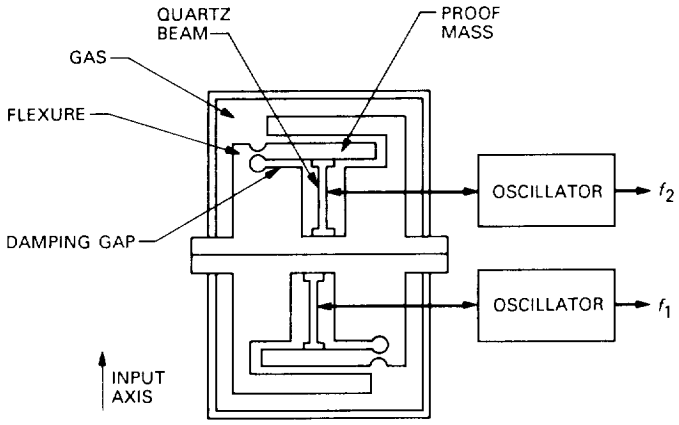

Fig. 14. A vibrating-beam accelerometer. Acceleration of the proof mass places one beam in tension and the other in compression. Acceleration is sensed as a change in the resonant vibrational frequency of the quartz beams.

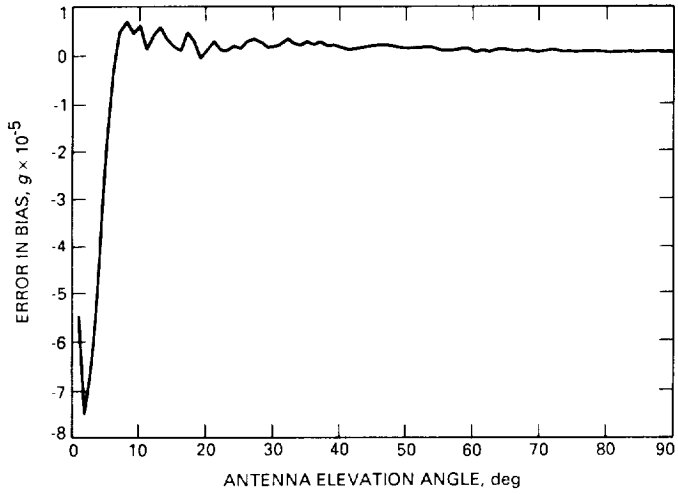

Fig. 15. Convergence of accelerometer bias estimate using an extended Kalman filter to estimate parameters. The antenna is elevated by 90 deg to provide maximum ease of identification.

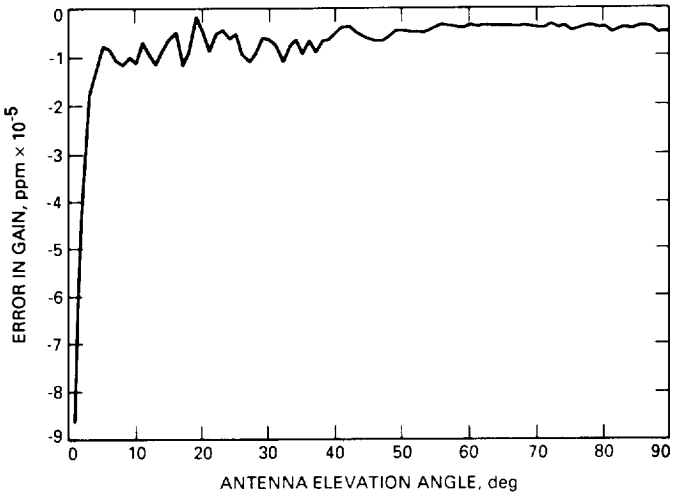

Fig. 16. Convergence of accelerometer gain estimate using an extended Kalman filter.

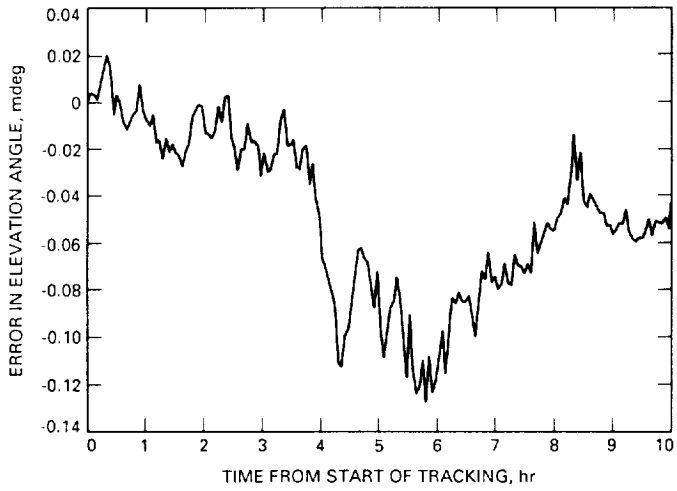

Fig. 17. Performance of a combined minimum-variance estimator and extended Kalman filter for estimating elevation angle during a 10-hr track of an inertially stationary object elevated 45 deg from Earth's equator.

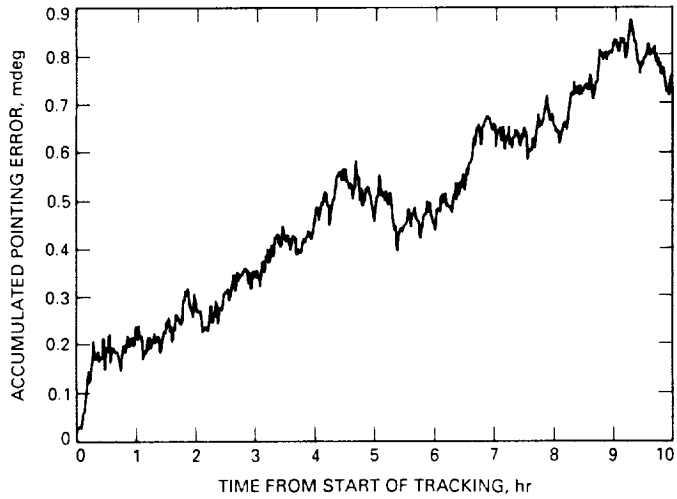

Fig. 18. Propagation of attitude errors obtained from three-axis gyroscope integration. Initial attitude error is set to zero.

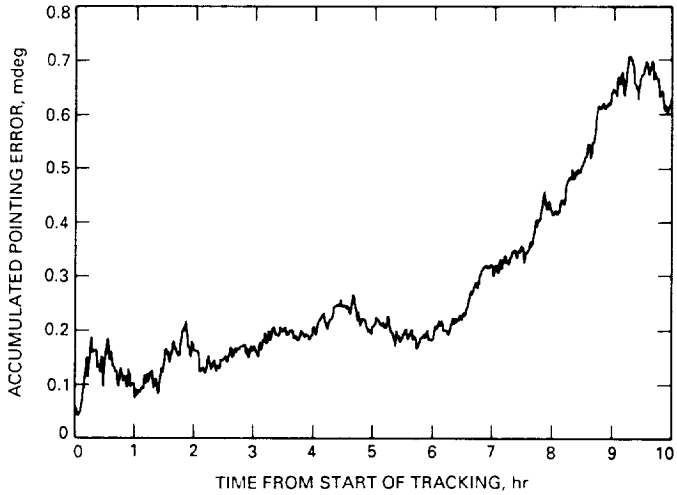

Fig. 19. Performance of attitude estimator that combines gyroscope integration with knowledge of local vertical. The additional information improves attitude accuracy.